

DOI: <https://doi.org/10.33103/uot.ijccce.24.3.7>

# Comparative Analysis of Two Robust Strategies for an Angular Velocity Control System

Aws M. Abdullah<sup>1</sup>, Hasan H. Ali<sup>2</sup>, Arif A. Al-Qassar<sup>3</sup>, Shibly A. Al-Samarraie<sup>4</sup><sup>1</sup> University of Baghdad, Baghdad, Iraq,<sup>2</sup> Directorate of Studies, Planning, and Follow-up, Ministry of Higher Education and Scientific Research, Baghdad, Iraq<sup>3,4</sup> Control and Systems Engineering Department, University of Technology, Baghdad, Iraq.<sup>1</sup>cse.21.01@grad.uotechnology.edu.iq, <sup>2</sup>hasan\_h2002@yahoo.com,<sup>3</sup>Arif.A.Alqassar@uotechnology.edu.iq, <sup>4</sup>dr.shiblyahmed@yahoo.com

**Abstract**— In this paper, a novel flow control strategy which is the inlet throttled pump was used to design an angular velocity control system for rotary actuator. Inlet throttled systems have good performance in addition to their high efficiency compared to traditional valve controlled systems. The flow in the proposed system is adjusted by a valve that is positioned at the pump inlet with the purpose of reducing the energy losses across the valve. This regulated flow is used then to control the actuator angular velocity. The system was modeled and the open loop stability and performance were studied. In order to improve the system performance, Robust-Proportional-Integral-Derivative (RPID) and structured singular value ( $\mu$ ) controllers have been designed. The multiplicative uncertainty was analyzed to assess the robustness of the feedback control system where six parameters were considered uncertain within a range of  $\pm 10\%$ . The robust stability and performance requirements of the closed-loop angular velocity control system were assessed in the frequency domain. The time response of the system showed that the system is stable with both (RPID) and ( $\mu$ ) controllers. The  $\mu$  controller can handle parametric uncertainty without requiring pure integral term which is a significant advantage over the (RPID) controller. On the other hand, the (RPID) controller could achieve robust performance, making it much suitable for systems that require high levels of performance and robustness. In summary, the the (RPID) and  $\mu$  controller is a more comprehensive solution for ensuring the best performance of a system. The results for each (RPID) and  $\mu$ -controllers showed no oscillations, zero percent overshoot. Each of the (RPID) and  $\mu$ -controllers meets the robustness needs.

**Index Terms**— Pump, valve, inlet throttling valve, angular velocity control, robust control,  $\mu$  synthesis, D-K iteration, RPID controller .

## I. INTRODUCTION

One of the power transmission systems is hydrostatic transmission, which uses pressurized hydraulic fluid to transfer mechanical energy. In contrast to traditional gear-based transmissions, hydrostatic transmissions offer smooth, step-less speed and torque control. Hydrostatic transmissions are common in machinery where precise movements, high low-speed torque, and frequent directional changes are needed. [1]

DOI: <https://doi.org/10.33103/uot.ijccce.24.3.7>

This paper proposes a new hydraulic closed-loop hydrostatic transmission system. As seen in *Fig. 1*, the proposed hydrostatic transmission system's major components are a throttling valve that regulates the pump flow rate, an inlet-throttled pump, and a rotary actuator. In order to minimize the energy losses across the pump, the throttling valve is positioned upstream of it [2]. The proposed system was designed to be robust regarding stability and performance requirements despite variations in operating conditions, uncertainties, and disturbances. [2,3]. Robust PID and Structured Singular Value Mu-controllers are proposed as robust controllers, where the robust PID contributed with enhancing performance under uncertainties, improving system stability, wider range of applications, reducing needs for returning, faster response times and reducing sensor requirements. The Mu-controllers contributed with robustness to uncertainties, superior performance in multivariable systems, guaranteed stability, broad applicability, systematic design approach and scalability [4,9].

Different papers investigated the use of the robust controllers to the hydraulic systems. [4] developed electrohydraulic power steering robust control system based on a 6-th order Mu-controller is presented. The analysis of robust stability and robust performance of developed control systems is performed. Results show that the control system will maintain its performance for a 25 percent larger uncertainty than the prescribed one. [5] presented depth controller design steps using the Mu-synthesis method for a small autonomous underwater vehicle (AUV), facing parametric uncertainties, with assumptions: instantaneous fin response, no underwater currents, and no sensor noises.

Robust performance and stability were assessed by the structured singular value Mu-synthesis for designing and analysis of Controller with PID structure for single input single output (SISO) plant [6], where this Controller is obtained via optimization of nominal closed-loop poles; these controllers are compared with the D-K iteration as a standard method for Mu-synthesis. [7] a preliminary application of V&V  $\mu$  analysis was introduced with a simple model of the Vega launcher as a case study, being successfully compared to the outcomes of MC and optimization-based tools. Vega is the European lightweight launch vehicle (LV) developed under the responsibility of the European Space Agency by ELV S.p.A. as the prime contractor. [8] Proposed and investigated a novel method for approximating structured singular values (Mu values). These quantities constituted an important tool in the stability analysis of uncertain linear control systems and structured eigenvalue perturbation theory.

In [9], A speed control system for a hydraulic motor was designed. A throttling valve along with a constant displacement pump was used as a means of flow adjustment. The system was modeled and stability and performance of the open loop and feedback system cases have been investigated. For the closed loop case, CPID and H-infinity controllers were considered and the frequency domain was adopted in the design process. The multiplicative parametric uncertainty was considered and the system robustness was assessed. The time response for the open and the feedback cases was determined and compared. [10] Proposed work to build a reliable, robust PID controller to tolerate the system sensor actuator failures of dynamic characteristics for TRMS of helicopter system. Presented robust PID controller, with  $H_\infty$  observer, which makes it reliable also. [11] Designed a robust PID controller in order to control an electro hydraulic actuator. The derived PID controller achieves precise positioning of the actuator piston in a wide range of physical uncertainties and external disturbances. The performance of the actuator variables is illustrated via simulations. [12] Presented a robust control strategy for the hydraulic servo-actuator. The robust control rule was created by utilizing Matlab/Simulink and Toolbox techniques to account for a variety of disturbances that can both destabilize and impair the operation of the closed-loop system. [13] discussed how to develop control systems utilizing the  $H_2$  and  $H_\infty$  robust control techniques. According to simulation results, the  $H_\infty$  controller ensures strong stability for the closed-loop system, whereas the  $H_2$  controller monitors a desired closed-loop performance. [14] Provide a swing leg system with strong controller synthesis and  $H_\infty$  loop shaping. This Controller ensures a fair balance between tracking accuracy and resilience in the

DOI: <https://doi.org/10.33103/uot.ijccce.24.3.7>

face of various model uncertainties and disruptions. The outcomes demonstrated that the system remained stable with 20% parametric uncertainty. [15] offered  $H_\infty$  and  $H_2$  optimum synthesis controllers to enhance the hydraulic machine's performance, where MATLAB/Simulink Toolbox was effectively used to study and simulate the design and operation of a tire changer machine with a hydraulic system. The uncertainty of the inflow metering of the Velocity Control System (VCS) was investigated in [16], where a proportional integral derivative (PID) and  $H_\infty$  were proposed to control the system. The results indicated that  $H_\infty$  and PID have the same performance, but  $H_\infty$  Controller satisfies the robustness criterion.

In the proposed model, the flow rate is controlled by the inlet throttling valve and a Fixed Displacement Pump (FDP). The stability and performance of the open and closed-loop situations were studied. Robust PID and Mu-controllers in the frequency domain were built for closed-loop operation. The system's robustness was assessed, and the multiplicative parametric uncertainty was examined. The paper computed and compared the temporal responses for both open- and closed-loop scenarios. The paper proposed firstly, the description of proposed hydrostatic transmission system. secondly, the description of dynamic mathematical model of the proposed system, thirdly analysis of the proposed system with and without uncertainties, fourthly design the robust controllers with uncertainties, as well as the analysis of results and the conclusions.

## II. DESCRIPTION OF THE SYSTEM

As shown in *Fig. 1*, The proposed hydrostatic transmission system utilizes an inlet throttling valve for controlling the flow. The inlet-throttled pump is proposed as the main part of this system because it has high performance effectiveness with respect to traditional valve-controlled systems. A fixed displacement pump pumps the flow at the desired pressure to the rotary actuator. The rotational mass-spring-damper system in *Fig. 1* represents the hydrostatic transmission load that is changing its position by the actuator, and  $T_d$  shows the load disturbance torque. The symbols ( $b$ ), ( $k$ ), and ( $J$ ) in *Fig. 1* represent the viscous damping coefficient for the load, torsional spring rate, mass moment of inertia, and respectively.

The rotary actuator is directly coupled to the Mass rotating at the output shaft and is depicted with a volumetric displacement fixed for every rotation,  $V_a$ . The fixed displacement pump is rotating at an angular velocity of  $\omega_p$  using a power source (not depicted in *Fig. 1*) and is scaled based on its volumetric displacement,  $V_p$ , as illustrated in *Fig. 1*. The supply line pressure of the charge pump is controlled by a relief valve of high-pressure called  $P_{in}$ , which is adjusted at the desired pressure of the supply. The primary fixed-displacement pump receives makeup flow from the charge pump, a fixed-displacement pump that is coupled to the relief valve. It is often a gear pump or a gerotor pump. It is also possible for the system's flow passageways to direct fluid flow into the reservoir for filtering and cooling. *Fig. 1* does not show the Coolers and filters. The hydraulic circuit's high-pressure side often operates at pressures more than 10 times  $P_c$ , or around 2 MPa.

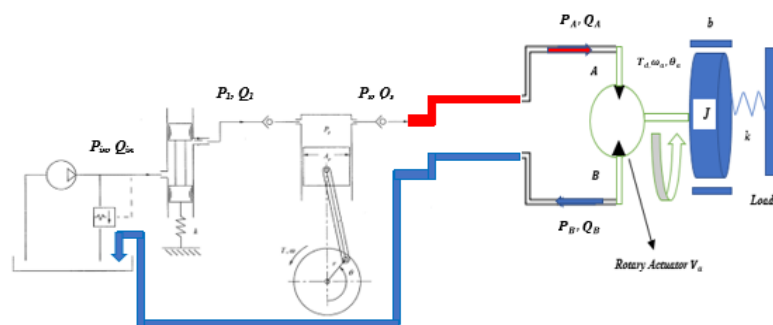


FIG. 1. ANGULAR VELOCITY CONTROL SYSTEM FOR A ROTARY ACTUATOR.

DOI: <https://doi.org/10.33103/uot.ijccce.24.3.7>

### III. DYNAMIC MODEL OF THE SYSTEM

The system's mathematical formulas are derived and non-dimensionalized. They comprise pressure dynamics as the equation for the rate of pressure increase and torque dynamics as the motion equation of the rotary actuator. The model has just one disturbance ( $T_d$ ) and one input ( $u$ ). The expression of the torque dynamics is given by [17,18] as shown in eq.(1):

$$J\ddot{\theta} + b\dot{\theta} + k\theta = \eta_{at}V_a(P_A - P_B) - T_d \quad (1)$$

where:

$P_A$  : The input fluid pressures of the actuator.

$P_B$  : The output fluid pressures of the actuator.

$T_d$ : Disturbance Torque

$V_a$ : Volumetric displacement of the actuator

$\eta_{at}$ : Efficiency of the actuator torque

$J$ : Moment of inertia of the Mass

$b$ : Viscous Damping Coefficient

$\theta$ : angular displacement

$\dot{\theta}$ : angular velocity

$\ddot{\theta}$ : angular acceleration

Let  $\dot{\theta} = \omega$

$P_s = P_A - P_B$ , let  $P_s = P_A$

Assuming the directional valve opening is wide enough, there are no restrictions on flow, resulting in small pressure drops through the valve passages and the directional control valve.

The torque that the rotary actuator applies to the load in Eq. (1) is given by  $\eta_{at}V_a(P_A - P_B)$  where  $\eta_{at}$  is the actuator torque efficiency.

For steady-state conditions:  $\dot{\omega} = 0$ ;  $\dot{T} = 0$ ;  $\dot{P}_s = 0$ ;

The rotor actuator is  $\omega = \dot{\theta}$ , and by setting  $k=0$ , the load spring is often removed from the analysis of the velocity control [18].

$$J\ddot{\theta} + b\dot{\theta} = \eta_{at}P_sV_a - T_d \quad (2)$$

The rate of pressure rise equation can be expressed as:

$$\frac{V}{\beta}\dot{P}_s + k_1P_s = (Q_i - V_a\dot{\theta}) \quad (3)$$

$V = V_0 + V_a\hat{\theta}$  : instantaneous volume of the chamber

Where  $\hat{\theta} = 2\pi*(1-\cos((180/\pi)*\theta))/2$

$V_0$ : The chamber volume at  $\theta$  equals to zero

$\beta$ : elasticity bulk modulus for the fluid

$Q_i$  : charge pump volumetric flow rate

$k_1$  : Coefficient of leakage

$V_a$ : Volumetric displacement per unit of rotation

$$\dot{P}_s = \frac{\beta}{V_0 + V_a\hat{\theta}}(Q_i - k_1P_s - V_a\dot{\theta}) \quad (4)$$

The pressure rise rate equation can be made simpler by linearizing it under the following nominal conditions:

$$\dot{\theta}_0 = Q_{i0} = P_{s0} = 0 \quad (5)$$

In its linear version, the equation for the pressure rise rate is as follows:

DOI: <https://doi.org/10.33103/uot.ijccce.24.3.7>

$$\dot{P}_s = \frac{\beta}{V_o} (Q_i - k_1 P_s - V_a \dot{\theta}) \quad (6)$$

The following is an expression for the inlet flow,  $Q_{in}$ :

$$Q_i = A_v C_d \sqrt{\frac{2P_i}{\rho}} \quad (7)$$

At the operational point, the nonlinear mathematical model is linearized. following that, non-dimensionlization can simplify and generalize the linearized mathematical model [19]. as shown in eq. (2) and eq. (6) using the following reference conditions:

$$\begin{aligned} P_s &= \hat{P}_s P_{Sr} \\ \omega_a &= \hat{\omega}_a \omega_{ar} \\ A_v &= \hat{A}_v A_r \\ P_i &= \hat{P}_i P_{ir} \\ t &= \hat{t} \tau \end{aligned} \quad (8)$$

where  $\tau$  is the time constant.

The linearized model is scaled to provide output, disturbance, and input at roughly the same magnitude. To do this, divide each variable by the greatest change possible. That is, the dimensionless equations that are produced can be written like this:

$$\frac{d(\hat{P}_s P_{Sr})}{d(\hat{t} \tau)} = \frac{\beta}{V_o} \left( A_r C_d \sqrt{\frac{2P_{ir}}{\rho}} \hat{A}_v \sqrt{\hat{P}_i} - k_1 \hat{P}_s P_{Sr} - V_a \hat{\omega}_a \omega_{ar} \right) \quad (9)$$

Multiply eq. (9) by  $\tau/P_{Sr}$

$$\dot{\hat{P}}_s = \frac{\tau \beta}{V_o P_{Sr}} A_r C_d \sqrt{\frac{2P_{ir}}{\rho}} \hat{A}_v \sqrt{\hat{P}_i} - \frac{\tau \beta}{V_o} k_1 \hat{P}_s - \frac{\tau \beta \omega_{ar}}{V_o P_{Sr}} V_a \hat{\omega}_a \quad (10)$$

$$\text{Let } \tau = \frac{V_o}{\beta k_1} \quad (11)$$

Substituting eq. (11) into eq. (10) gives:

$$\dot{\hat{P}}_s = \frac{V_o}{\beta k_1} \frac{\beta}{V_o P_{Sr}} A_r C_d \sqrt{\frac{2P_{ir}}{\rho}} \hat{A}_v \sqrt{\hat{P}_i} - \frac{V_o}{\beta k_1} \frac{\beta}{V_o} k_1 \hat{P}_s - \frac{V_o}{\beta k_1} \frac{\beta \omega_{ar}}{V_o P_{Sr}} V_a \hat{\omega}_a \quad (12)$$

In the end, the non-dimensional pressure increase equation may be expressed like this:

$$\dot{\hat{P}}_s + \hat{P}_s = \xi_1 \hat{A}_v \sqrt{\hat{P}_i} - \xi_2 \hat{\omega}_a \quad (13)$$

Dimensionless groups  $\xi_1$  and  $\xi_2$  are given in eqs. (14) and (15), respectively.

$$\xi_1 = \frac{A_r C_d \sqrt{\frac{2P_{ir}}{\rho}}}{P_{Sr} k_1} \quad (14)$$

$$\xi_2 = \frac{\omega_a V_a}{k_1 P_{Sr}} \quad (15)$$

Similarly, the Equation for non-dimensional motion may be obtained as follows:

$$\int \frac{d(\hat{\omega}_a \omega_{ar})}{d(\hat{t} \tau)} + \hat{b} \hat{\omega}_a \omega_{ar} = \eta_{at} \hat{P}_s P_{Sr} V_a - \hat{T}_d \quad (16)$$

The motion equation can be stated in its dimensionless version by dividing it by  $\eta_{at} P_{Sr} V_a$  in equation (16).

$$\hat{J} \hat{\omega}_a + \hat{b} \hat{\omega}_a = \hat{P}_s - \hat{T}_d \quad (17)$$

where

$$\begin{aligned} \hat{J} &= \frac{J \omega_{ar}}{\eta_{at} P_{Sr} V_a \tau} \\ \hat{b} &= \frac{b \omega_a}{\eta_{at} P_{Sr} V_a} \\ \hat{V}_a &= \frac{V_a}{V_a} = 1 \end{aligned} \quad (18)$$

DOI: <https://doi.org/10.33103/uot.ijccce.24.3.7>

$$\hat{T}_d = \frac{\hat{T}_d}{\eta_{at} P_{sr} V_a}$$

The following may be done to rearrange eqs. (13) and (17) in state-space matrix form:

$$\begin{aligned} \dot{x} &= Ax + Bu + Dd(t) \\ y &= Cx \end{aligned} \quad (19)$$

$$\begin{aligned} x &= [\hat{P}_s \quad \hat{\omega}_a]^T \\ u &= \hat{A}v \\ y &= \hat{\omega} \\ \dot{x}_1 &= -x_1 - \xi_2 x_2 + \xi_1 \sqrt{\hat{P}_i} u_1 \\ \dot{x}_2 &= \frac{1}{j} x_1 - \frac{\hat{b}}{j} x_2 - \frac{1}{j} u_2 \\ y &= x_2 \end{aligned} \quad (20)$$

$$A = \begin{bmatrix} -1 & -\xi_2 \\ \frac{1}{j} & -\frac{\hat{b}}{j} \end{bmatrix} \quad B = \begin{bmatrix} 0 \\ -\frac{1}{j} \end{bmatrix} \quad D = \begin{bmatrix} \xi_1 \sqrt{\hat{P}_i} \\ 0 \end{bmatrix} \quad C = [0 \quad 1] \quad (21)$$

In this work, the stability of the open loop system was ascertained using the Routh-Hurwitz stability criterion. The characteristic Equation's coefficients must all be positive in order to meet this requirement. The following describes how the Routh-Hurwitz stability criteria are put into practice:

$$\det(sI - A) = s^2 + \left(\frac{\hat{b}}{j} + 1\right)s + \left(\frac{\hat{b} + \xi_2}{j}\right) = 0 \quad (22)$$

$$a_0 = 1 > 0$$

$$a_1 = \left(\frac{\hat{b}}{j} + 1\right) > 0$$

$$a_2 = \left(\frac{\hat{b} + \xi_2}{j}\right) > 0$$

A stable open system is indicated by all of the characteristic Equation's coefficients being larger than zero. Equations (23) and (24) were produced, illustrating how the mathematical model was converted into transfer functions. The input valve opening area and the motor's output angular velocity transfer function are as follows:

$$G_P = \frac{\hat{\omega}_A}{\hat{A}v} = \frac{\xi_1 / j}{s^2 + \left(\frac{\hat{b}}{j} + 1\right)s + \left(\frac{\hat{b} + \xi_2}{j}\right)} \quad (23)$$

The system's transfer function connects the motor's output angular velocity to the input disturbance torque:

$$G_d = \frac{\hat{\omega}_d}{\hat{T}_d} = \frac{-\frac{s+1}{j}}{s^2 + \left(\frac{\hat{b}}{j} + 1\right)s + \left(\frac{\hat{b} + \xi_2}{j}\right)} \quad (24)$$

Equation (27) displays the transfer function for the inlet throttling valve dynamics obtained by experimentation.

$$G_v(s) = \frac{\hat{A}_v}{\hat{V}_{in}} = \frac{\hat{k}_v e^{-s\hat{t}_d} \hat{\omega}_n^2}{s^2 + 2\xi \hat{\omega}_n s + \hat{\omega}_n^2} \quad (25)$$

As seen in non-dimensional bandwidth frequency, the time delay may enclose the closed-loop bandwidth frequency  $\omega_b$  [19,20]:

$$\hat{\omega}_b < \frac{1}{\hat{t}_d} \quad (26)$$

Equation (27) shows the complete system dynamics transfer function.

$$G(s) = G_v(s)G_P(s) \quad (27)$$

DOI: <https://doi.org/10.33103/uot.ijccce.24.3.7>

Table I lists the nondimensional quantities mentioned in eq. (23) and eq. (25).

TABLE I. LIST OF NONDIMENSIONAL QUANTITIES VALUES

Quantity	Values	Quantity	Values
$\hat{f}$	5.84	$\xi_2$	8.89
$\hat{b}$	0.15	$\hat{\omega}_n$	5.31
$\hat{T}$	1	$\xi$	0.8
$\hat{R}$	1	$\hat{t}_d$	0.24
$\eta_{at}$	0.95	$\hat{k}_v$	1.214
$\xi_1$	10		

#### IV. CONTROLLER DESIGN AND UNCERTAINTY ANALYSIS

The usual optimization controller synthesis approach [22] was used to develop the transfer function  $\mu$  and robust controllers. As shown in Fig. 2, these resilient controllers can minimize the system transfer function matrix with external inputs and outputs ( $\hat{R}$  and  $\hat{T}_d$ ), and ( $z_1$  and  $z_2$  norms) respectively.

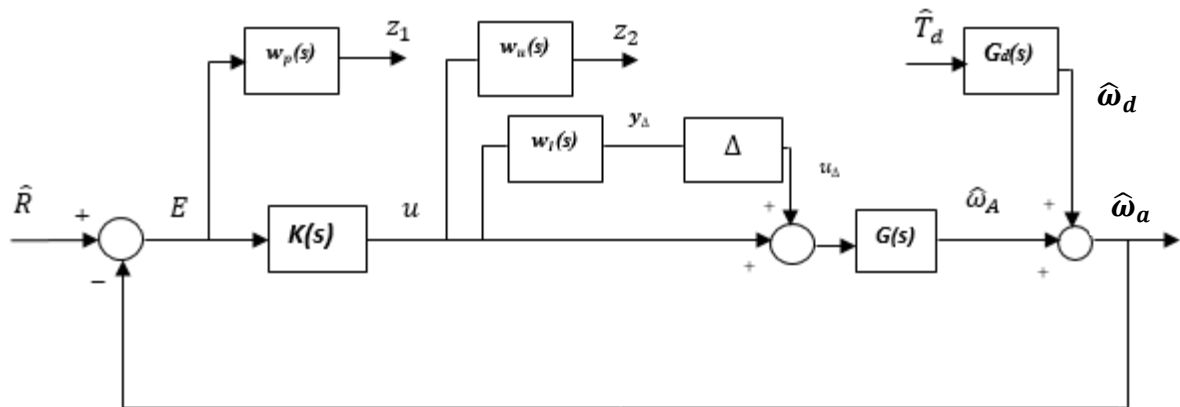


FIG. 2. THE BLOCK DIAGRAM OF THE SYSTEM INCLUDING THE WEIGHTS.

As seen in Fig. 3, the function of sensitivity  $S$  is the reference signal ( $\hat{R}$ ) transfer function to the error signal ( $E$ ) and may be expressed as stated in eq. (28).

$$S(s) = \frac{E(s)}{\hat{R}(s)} \frac{1}{1+G(s)G_c(s)} \tag{28}$$

The following is the textual influence of the disturbance on the error signal transfer function:

$$\frac{E(s)}{\hat{T}_d(s)} = -S(s) \cdot G_d(s) \tag{29}$$

Frequency-dependent weighting functions are the control effort weight ( $w_u$ ) and the performance weight ( $w_p$ ). The performance weight is related to performance requirements; it is used to reflect the requirements on the shape of the output sensitivity function.

DOI: <https://doi.org/10.33103/uot.ijccce.24.3.7>

The weighting control function ( $w_u$ ) is an upper bound for the controller gain. It reflects some restrictions on the control signal compromise between the conflicting objectives.

The temporal delay of the valve was estimated using a first-order Padé approximation. Over a known range, the total system dynamics took the parameter fluctuations into account. In order to investigate the multiplicative uncertainty, the perturbed plants will be generated by the prior transfer functions. Equation (30) illustrates the multiplicative uncertainty model of the perturbed plants, whereas equation (31) shows the uncertainty weight,  $w_I$ .

$$l_I(\omega) = \max_{G_{pert}(j\omega) \in \Pi} \left| \frac{G_{pert}(j\omega) - G(j\omega)}{G(j\omega)} \right| \quad (30)$$

$$w_I(j\omega) \quad G_{pert} \in \Pi \quad (31)$$

Six unknown factors were taken into consideration to analyze the multiplicative uncertainty. The valve dynamics have four unknown parameters: natural frequency, static gain, time delay, and damping ratio. These parameters are within  $\pm 10\%$  of their nominal value. As per eq. (31), the value of  $w_I$  ought to be greater than the biggest inaccuracy  $l_I(\omega)$  that transpires throughout the frequency domain.

The numerical computation of the hypothetical plant  $G(j\omega)$  and its perturbations  $G_{pert}(j\omega)$  yielded an upper bound for the multiplicative error in eq. (32), for various frequency domains. The uncertainty weight transfer function,  $w_I$ , stated in eq.(32), where eq. (32) has the upper bound on the uncertainty, shown in red in Fig. 6.

$$w_I(s) = \frac{1.056s^2 + 12.47s + 27.92}{s^2 + 11.68s + 26.87} \quad (32)$$

#### A. Closed-Loop System Interconnections With Uncertainty

Based on the block diagram of Fig. 2, the equations of  $y_\Delta$ ,  $z_1$ ,  $z_2$ , and  $E$  may be written as follows,

$$y_\Delta = w_I u \quad (33)$$

$$z_1 = -G w_P u_\Delta + w_P \hat{R} - G_d w_P \hat{T}_d - G w_P u \quad (34)$$

$$z_2 = w_u u \quad (35)$$

$$E = -G u_\Delta + I \hat{R} - G_d \hat{T}_d - G u \quad (36)$$

As seen in eq. (37), eqs. (37–40) are stated in matrix form.

$$\begin{bmatrix} y_\Delta \\ z \\ E \end{bmatrix} = [P] \begin{bmatrix} u_\Delta \\ \omega \\ u \end{bmatrix} \quad (37)$$

Eq. (38) specifies the exogenous inputs ( $w$ ) and outputs ( $z$ ).

$$w = \begin{bmatrix} \hat{R} \\ \hat{T}_d \end{bmatrix} \quad z = \begin{bmatrix} z_1 \\ z_2 \end{bmatrix} \quad (38)$$

Equation (39) illustrates the P matrix, whereas Equation (40) provides the constituents of the P matrix, namely P11, P12, P21, and P22.

$$P = \begin{bmatrix} P11 & P12 \\ P21 & P22 \end{bmatrix} \quad (39)$$

DOI: <https://doi.org/10.33103/uot.ijccce.24.3.7>

$$P_{11} = \begin{bmatrix} 0 & 0 & 0 \\ -Gw_p & w_p & -G_d w_p \\ 0 & 0 & 0 \end{bmatrix}, P_{12} = \begin{bmatrix} w_I \\ -Gw_p \\ w_u \end{bmatrix}, P_{21} = [-G \quad 1 \quad -G_d], P_{22} = [-G] \quad (40)$$

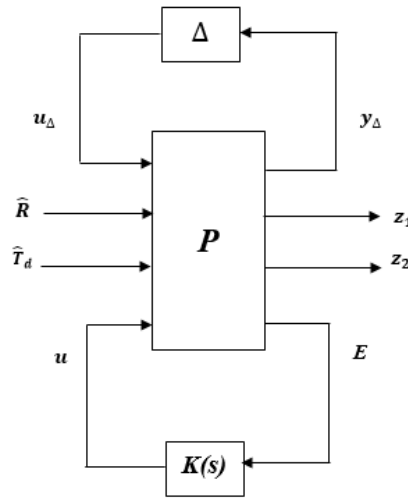


FIG. 3. THE OVERALL SETTING OF THE CONTROLLER (FOR CONTROLLER SYNTHESIS).

**B.  $\mu$  - Synthesis**

The definition of the structured matrix  $\hat{\Delta}$  is provided in

$$\hat{\Delta} = \begin{bmatrix} \Delta & 0 \\ 0 & \Delta_p \end{bmatrix} \quad (41)$$

As an output from ( $N$ ), the uncertainty model ( $\Delta$ ) has a linked input ( $y_\Delta$ ), as seen in Fig. 5 It will use its output ( $u_\Delta$ ) as an input for ( $N$ ). While two of the outputs ( $z_1$  and  $z_2$ ) of the performance uncertainty model ( $\Delta_p$ ) are driven from the output of ( $N$ ), the other two outputs ( $\hat{R}$  and  $\hat{T}_d$ ) will be used as inputs to ( $N$ ).

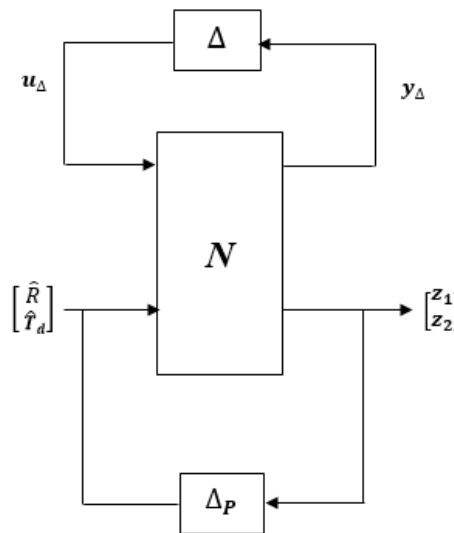


FIG. 4. THE  $N - \Delta$  STRUCTURE.

The nominal matrix of the system,  $N$ , as seen in Fig. 4, may be expressed as follows:

$$N = P_{11} + P_{12}K(I - P_{22})^{-1}P_{21} \quad (42)$$

Eq. (43) illustrates how the matrix  $N$  is related to its inputs and outputs.

DOI: <https://doi.org/10.33103/uot.ijccce.24.3.7>

$$\begin{bmatrix} y_{\Delta} \\ z_1 \\ z_1 \end{bmatrix} = [N] \begin{bmatrix} u_{\Delta} \\ \hat{R} \\ \hat{T}_d \end{bmatrix} \quad (43)$$

It is possible to divide an N matrix using the performance and stability criteria into (N11, N22, N21, and N22):

**Nominal stability (N.S.):** the system is stable regardless of the uncertainties.

**Nominal performance (N.P.):** According to eq. (44) This performance happens when the nominal system is in the stability region and meets the performance requirements notwithstanding uncertainties.

$$N.P. \Leftrightarrow \|N_{22}\|_{\infty} < 1 \quad (44)$$

**Robust Stability (R.S.):** the system is in the stable region regarding uncertainties, as illustrated in eq. (45).

$$R.S. \Leftrightarrow \|N_{11}\|_{\infty} < 1 \quad (45)$$

**Robust performance:** As shown in eq. (46), it is met when the system achieves the performance criterion for all uncertainty-set perturbed plants while maintaining nominal stability.

$$RP \Leftrightarrow \mu(N, \hat{\Delta}) < 1 \quad (46)$$

TABLE II. DIMENSIONAL QUANTITY DEFINITIONS

Dimensional Quantity	NOMENCLATURE	Units
$A_v$	the Inlet Throttling Valve Opening Area	$m^2$
$b$	The Damping Coefficient of the Viscous	$kg.m^2/s$
$T_d$	Disturbance Torque	$N.m$
$R$	Disired velocity	$rad/s$
$k_s$	static gain of the valve	-----
$k_1$	Coefficient of the Leakage	$m^4.s/kg$
$k_v$	Static Gain of the Valve	$m^2/volt$
$P_s$	Pressure Supply	$N/m^2$
$J$	moment of inertia of the Mass	$kg.m^2$
$cd$	Discharge Coefficient	-----
$t_d$	Time Delay of the Valve	$s$
$V_o$	Volume of the Actuator	$m^2$
$V_a$	Volumetric displacement of the actuator	$m^3/rad$
$\rho$	fluid density	$kg/m^3$
$\eta_{at}$	Efficiency of the Actuator	-----
$\beta$	Bulk Modulus of the Fluid	$N/m^2$
$\omega_n$	Natural Frequency of the Valve	$rad/s$
$P_i$	input pressure	$N/m^2$
$\xi$	The Damping Ratio of the Valve	-----
$\xi_1$	Group of non-dimensional	-----
$\xi_2$	Group of non-dimensional	-----

DOI: <https://doi.org/10.33103/uot.ijccce.24.3.7>

## V. ROBUST PID CONTROLLER DESIGN

The robust PID controller is a popular feedback controller in the closed-loop in industrial systems. The difference between a measured process variable and a desired set point is used to determine an error value. It modifies the procedure using the terms derivative, integral, and proportional. The system's transfer function connects the disturbance of the input torque and the motor's angular velocity. The search method employed in this study to locate values for the  $K_p$ ,  $K_i$ , and  $K_d$  parameters that are almost ideal is called particle swarm optimization (PSO) [21]. The best solution among all workable solutions is represented by the values of the derivative, integral, and proportional terms found in this work:  $K_d = 0.0901$ ,  $K_i = 0.153$ , and  $K_p = 0.01$ . The PID controller transfer function will be as eq. (47)

$$K(s) = \frac{U(s)}{E(s)} = (K_p + \frac{K_i}{s} + K_d s). \quad (47)$$

The objective function that it is desired to minimize will be  $\| |W_p S| + |W_I T| \|_{\infty}$

$$\text{The objective function} = \| |W_p S| + |W_I T| \|_{\infty} < 1 \quad (48)$$

Where  $|W_p S| < 1$ ,  $|W_I T| < 1$ ,  $|W_u K S| < 1$

Equation (49) generates the sensitivity frequency response transfer function upper restrictions, which inverse the performance weight [23,24].

$$w_p = \frac{\frac{s}{M} + \hat{\omega}_b}{s + a\hat{\omega}_b} \quad (49)$$

With a low-frequency error of  $a=10e-4$  and a high-frequency error of  $M=1$ , the non-dimensional bandwidth frequency is  $\hat{\omega}_b = 0.1053$ . To guarantee a suitably modest steady-state inaccuracy, a gain of 0.1 was used. Although the transient response have high speed, a bigger gain results in fewer steady-state errors. In a non-dimensional model in which the input is normalized to its highest value, the control effort weight ( $w_u$ ) is usually set to one as shown in Fig. 2, [25].

the Routh-Hurwitz criterion is employed to test the stability of the closed-loop system. If the Routh-Hurwitz criterion fails with the resulting parameters, the particle can not be used as a candidate solution.

The design procedures of the PSO-based robust PID controller can be summarized as follows:

The Routh-Hurwitz criterion is employed to test the stability of the closed-loop system. If the Routh-Hurwitz criterion fails with the resulting parameters, the particle cannot be used as a candidate solution.

The design procedures of the PSO-based PID controller can be summarized as follows:

Input: Initialize cost function, upper bound ( $ub$ ), lower bound ( $lb$ ), Population size ( $N$ ), initial velocity ( $v$ ), initial position ( $x$ ), Inertia weight ( $\theta$ ), maximum and minimum inertia weights ( $\theta_{max}$  and  $\theta_{min}$ ), number of iterations ( $T_{max}$ ), uniformly distributed random number in the range (0,1) ( $r_1$  and  $r_2$ ), individual and social cognitive ( $C_1$  and  $C_2$ )

Step 1. Randomly initialize the positions and velocities of particles using uniform probability distribution.

Step 2. Return to Step 1 until the Routh-Hurwitz stability test is satisfied.

Step 3. Calculate the cost of each particle using special cost function.

Step 4. Compare each particle's current cost with its  $P_{best}$ . If it is better, set the current value as the new  $P_{best}$ .

Step 5. Compare the best cost among the entire particle with  $G_{best}$ . If the current value is better, set the current best value as  $G_{best}$ .

Step 6. Calculate the particle's velocity by Eq. (4.54).

$$\theta = \theta_{max} - \left( \frac{\theta_{max} - \theta_{min}}{T_{max}} \right) t \quad (50)$$

DOI: <https://doi.org/10.33103/uot.ijccce.24.3.7>

$$v_i = \theta v_i(t-1) + c_1 r_1(p_{best,i} - x_i(t-1)) + c_2 r_2(g_{best,i} - x_i(t-1)) \quad (51)$$

Step 7. Recalculate the position of the particles by

$$x_i(t) = x_i(t-1) + v_i(t) \quad (52)$$

Step 8. Return to Step 2 until the maximum iterations or minimum error bound is attained.

The PID controller transfer function will be as eq. (53)

$$K(s) = \frac{U(s)}{E(s)} = (0.01 + \frac{0.153}{s} + 0.0901s) \quad (53)$$

## VI. MU- CONTROLLER DESIGN

A structured singular value (SSV) controller is a design technique used in control theory, specifically for robust control. It helps ensure a system remains stable and performs well even under uncertainties. The Structured Singular Value ( $\mu$ ) is a mathematical concept that quantifies the robustness of a control system to uncertainties. SSV controllers leverage a mathematical concept called the  $\mu$ -value. The  $\mu$ -value tells you how sensitive a system is to uncertainties within a specific structure. Imagine a box representing all possible uncertainties your system might encounter. The  $\mu$ -value tells you how much you can "stretch" the box (increase the uncertainties) before the system becomes unstable. SSV controllers offer a powerful approach to designing robust control systems. By explicitly considering uncertainties, they ensure systems perform well even in unpredictable environments.

The Mu-controller design steps use one of the iterative  $\mu$ -synthesis methods for the rotary actuator Inlet throttling angular velocity model. The D-K iteration method tests the Controller's stability and performance. The Controller was designed in the face of parametric uncertainties and disturbances, and the frequency domain is used to represent robust stability and performance for the proposed system.

The sensitivity transfer function upper bounds on the frequency response are inversely related to the performance weight, derived using eq. (54) [23,24].

$$w_p = \frac{\frac{s}{M} + \hat{\omega}_b}{s + a\hat{\omega}_b} \quad (54)$$

The non-dimensional bandwidth is  $\hat{\omega}_b = 0.15$ , with an error at the high frequency of  $M=4$  and an error at the low frequency of  $a=10e-3$ . In order to guarantee a suitably modest steady-state error, a gain of 0.7 was used. Although the transient response is poorer, a bigger gain results in fewer steady-state errors. In a non-dimensional model in which the input is normalized to its highest value, Typically, the effort weight of control ( $w_u$ ) is chosen to be 1, as shown in Fig. 2 [25].

As eq.(55) indicated, the Mu-controller transfer function was estimated using the Matlab function dksyn.

$$K(s) = \frac{0.1009 s^6 + 0.03111 s^5 + 0.0001823 s^4 + 1.061e-05 s^3 + 3.107e-10 s^2 + 9.585e-16 s + 9.53e-22}{s^7 + 0.2523 s^6 + 0.001544 s^5 + 8.725e-05 s^4 + 1.353e-08 s^3 + 7.217e-14 s^2 + 1.381e-19 s + 9.529e-26} \quad (55)$$

According to the D-K iteration approach in  $\mu$ -Synthesis, To indicate that P and K constitute N, the matrix N is expressed as  $N(P, K)$ . For the Robust Stability Robust Performance (RSRP) design, it is required to find a stabilizing controller K such that:

$$\sup_{\omega \in \mathbf{R}} \mu [N(P, K)(j\omega)] < 1 \quad (56)$$

For the "optimal" RSRP design, the objective is to solve for K

$$\inf_{\mathbf{K}(s)} \sup_{\omega \in \mathbf{R}} \mu [N(P, K)(j\omega)] \quad (57)$$

DOI: <https://doi.org/10.33103/uot.ijccce.24.3.7>

In [25], an iterative approach to solving eq. (56) was suggested. The D–K iteration  $\mu$ -synthesis approach is based on solving the following optimization problem for a diagonal constant scaling matrix  $D$  and a stabilizing controller  $K$ :

$$\inf_{K(s)} \sup_{D \in \mathcal{D}} \inf_{\omega \in \mathcal{R}} \bar{\sigma} [DN(P,K)D^{-1}(j\omega)] \quad (58)$$

Corresponding to the case of (56), A stabilizing controller is to be found such that

$$\sup_{\omega \in \mathcal{R}} \inf_{D \in \mathcal{D}} \bar{\sigma} [DM(P,K)D^{-1}(j\omega)] \quad (59)$$

The D–K iteration method is to alternately minimize (58), or to reduce the lefthand-side value of (59), for  $K$  and  $D$  in turn while keeping the other one fixed. For a given matrix  $D$ , either constant or transfer function, (58) is a standard  $H_\infty$  optimization problem

$$\inf_{K(s)} \|DM(P,K)D^{-1}\|_\infty \quad (60)$$

The iterative  $\mu$ -synthesis procedure for D–K is as follows:

Step 1: Make a first approximation for  $D$ , commonly putting  $D = I$ .

Step 2: Correct  $D$  and figure out  $K$ 's  $H_\infty$ -optimization.

$$K = \arg \inf_{K(s)} \|DF_t(P,K)D^{-1}\|_\infty \quad (61)$$

Step 3: After fixing  $K$ , resolve the convex optimization issue for  $D$  at every frequency within the chosen range of frequencies:

$$D(j\omega) = \arg \inf_{D \in \mathcal{D}} \|DF_t(P,K)D^{-1}(j\omega)\|_\infty \quad (62)$$

Step 4: Curve fit  $D(j\omega)$  to get a stable, minimum-phase  $D(s)$ ; return to Step 2 and repeat until the pre-specified maximum iteration number, a pre-specified convergence tolerance, or eq. (59) is attained.

The M-file is used to perform the Mu-synthesis. Table II displays the progress of the D-K iteration. An adequate controller is found after the fourth D-K cycle for the given situation. Table II shows that the optimal value of  $\mu$  is 0.978 following the fourth iteration. The M-file, which has the function `dkitopt` implemented, performs the  $\mu$ -analysis of the closed-loop system with a stable Mu-controller. The system could perform well and has strong stability.

## VII. ANALYSIS OF THE RESULTS

Equation (30) illustrates the multiplicative error resulting from design parameter changes across a frequency range in Fig. 6. This error is related to a rotary actuator's inlet throttling VCS. It can be seen that with the current range of parameter variation, there is uncertainty of about thirty three percent at low frequency, about fifty seven percent at medium frequency, and about forty seven percent at high frequency.

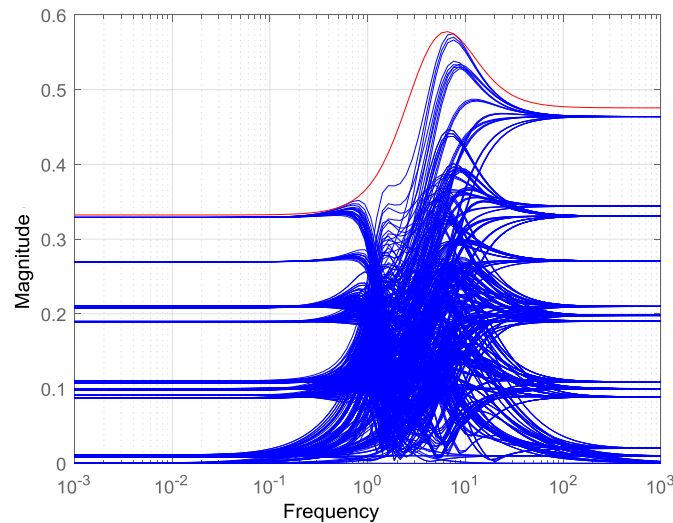
DOI: <https://doi.org/10.33103/uot.ijccce.24.3.7>

FIG. 6. BOUNDING THE GREATEST MULTIPLICATIVE ERROR USING THE MULTIPLICATIVE UNCERTAINTY TRANSFER FUNCTION.

Fig. 7 shows the system's temporal response for closed systems, using robust PID and Mu controllers for the disturbance and reference input. The 35-time constants were followed by the disturbance being introduced into the system ( $\hat{t}=35$ ). The input was a unit step. It is evident in percentage overshoot, steady-state error, disturbance rejection, and rise time. It is evident that the system with the robust PID and Mu – controllers has zero steady-state error, almost rejects the disturbance, and reaches the desired value again.

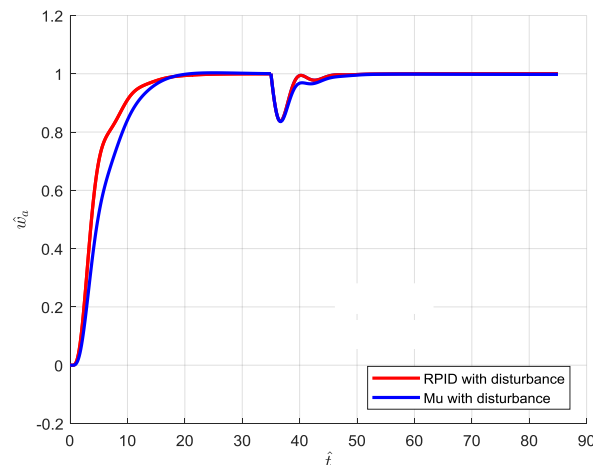


FIG. 7. THE TORQUE DISTURBANCES EFFECT ON THE TIME RESPONSE OF VELOCITY FOR BOTH CLOSED LOOP WITH RPID AND MU-CONTROLLERS.

The uncertain system with multiplicative uncertainty's temporal response is depicted in Fig. 8. The performance for the closed-loop system time response with controllers is close to each controller as the values of the changes of the uncertainties. Errors in the nominal system's uncertain parameters that fell between  $\pm 10\%$  of their nominal values were used to calculate the uncertainties, where it is noticed convergence between the robust PID controller and Mu-controller about response level with the uncertainties.

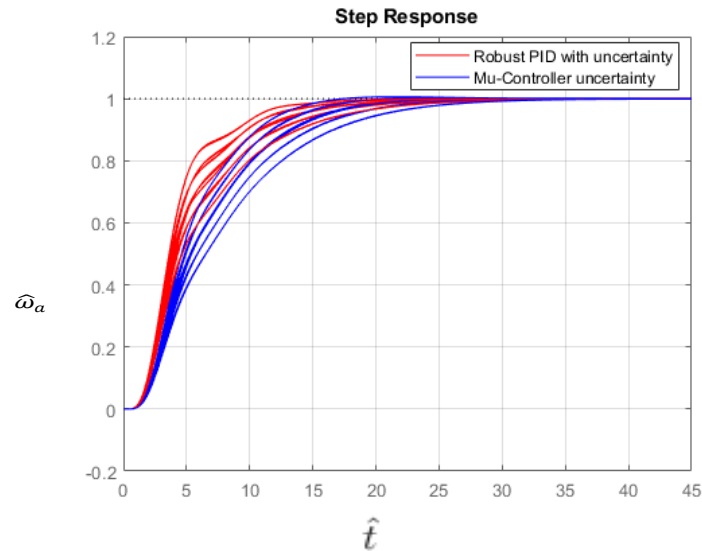
DOI: <https://doi.org/10.33103/uot.ijccce.24.3.7>

FIG. 8. THE CLOSED-LOOP VELOCITY TIME RESPONSE DISTURBED BY RPID AND MU CONTROLLERS.

The valve opening area represented the control action signal where, is plotted in Fig. 9 in the closed loop system with controllers where the effects of the disturbances are represented on the valve opening area in the Fig. 9 in the  $\hat{t}=35$  times where it is noticed increasing in the valve opening area level with the disturbance torque. It is shown the increasing in the valve opening area level of closed loop system with controllers, the RPID and Mu controllers are close.

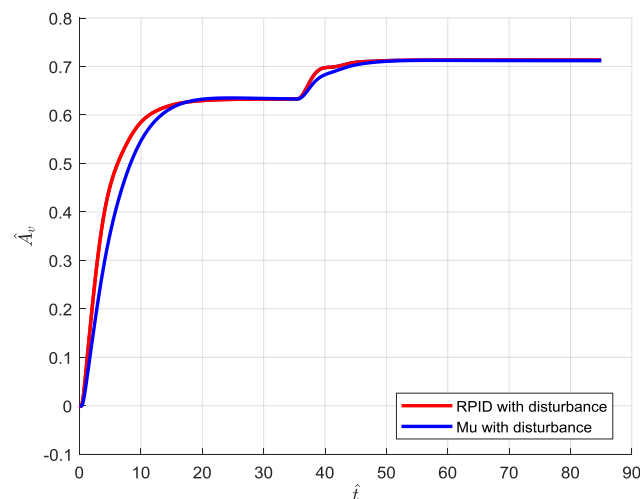


FIG. 9. THE VALVE OPENING AREA TIME RESPONSE FOR OPEN LOOP AND CLOSED-LOOP WITH RPID AND MU CONTROLLERS.

The conditions outlined in Equations (44–46) are shown in Fig. 10–12. The robust PID and Fig. 10 illustrate how Mu-controllers meet robust and nominal stability criteria, with each controller's  $\|N_{11}\|_\infty$  being smaller than 1 over the whole frequency range. Furthermore, as Fig. 11 illustrates, both controllers meet the nominal performance. Nevertheless, as Fig. 12 shows, both controllers meet the strong performance requirement, where all the requirements being smaller than 1 over the whole frequency range.

DOI: <https://doi.org/10.33103/uot.ijccce.24.3.7>

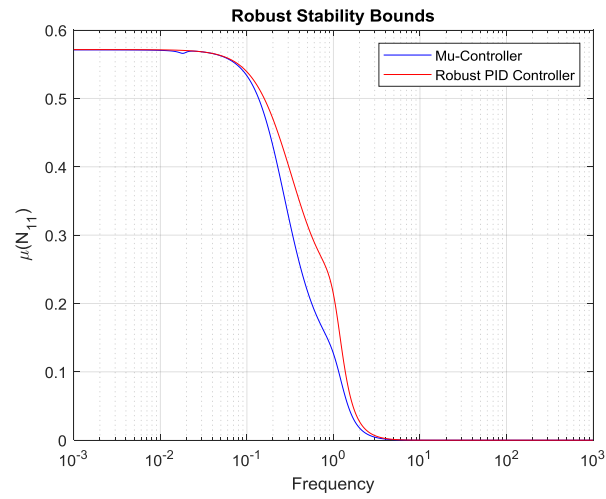


FIG. 10. THE REQUIREMENTS FOR THE ROBUST STABILITY.

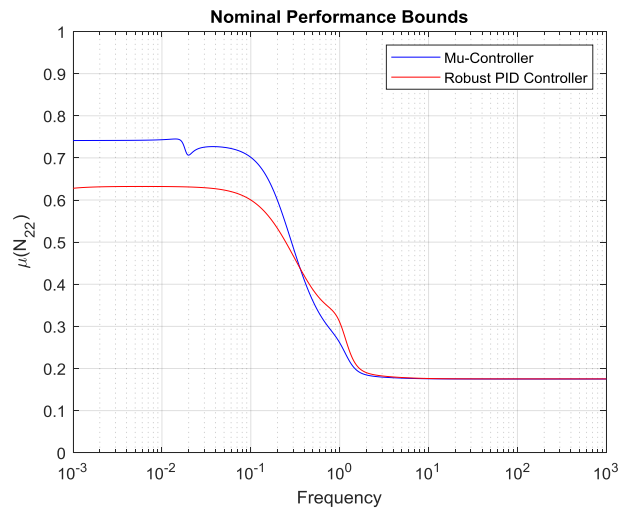


FIG. 11. THE REQUIREMENTS FOR THE NOMINAL PERFORMANCE.

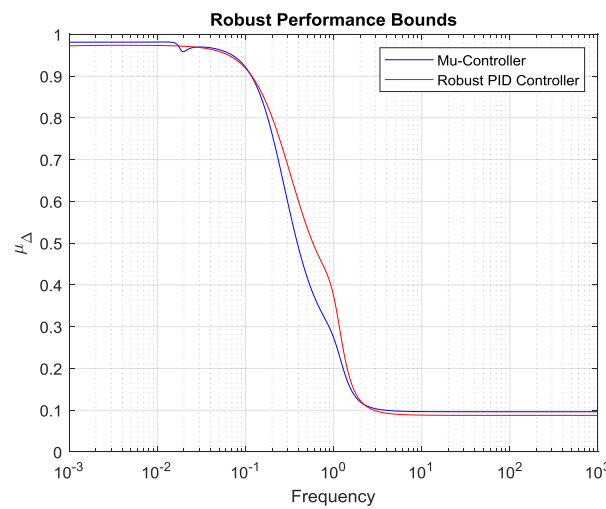


FIG. 12. THE REQUIREMENT FOR THE ROBUST PERFORMANCE.

DOI: <https://doi.org/10.33103/uot.ijccce.24.3.7>

All quantitative and numerical amounts are compared in Table III.

TABLE III. DIMENSIONAL QUANTITATIVE AND NUMERICAL COMPARISSION

System	Rise time	Over shoot	Error steady state	Oscillations	Control action	Nominal stability	Nominal performance (Maximum)	Robust stability (Maximum)	Robust performance (Maximum)
Closed Loop with Robust PID	0.625 s	zero	zero	No existing	5.862 $\times 10^{-6}$	stable	0.57 db For range ( $10^{-3}$ - $2 \times 10^{-2}$ )	0.625 db For range ( $10^{-3}$ - $1.7 \times 10^{-2}$ )	0.975 db For range ( $10^{-3}$ - $1.7 \times 10^{-2}$ )
Closed Loop with Structured Singular Value	0.78125 s	zero	zero	No existing	5.862 $\times 10^{-6}$	stable	0.57 db For range ( $10^{-3}$ - $2 \times 10^{-2}$ )	0.745 db ( $10^{-3}$ - $1.7 \times 10^{-2}$ )	0.978 db For range ( $10^{-3}$ - $1.7 \times 10^{-2}$ )

## VIII. CONCLUSIONS

In order to account for parametric uncertainty and disturbances, an inlet throttling velocity control system for a rotary actuator was built and examined in this study. Stability and performance were evaluated for feedback control and open-loop situations following system modeling. The Mu-controller and robust PID were used in the closed-loop architecture. Three scenarios were analyzed and contrasted regarding the system's robust stability and performance (open loop system, closed loop with robust controllers). The simulation results explained that both the Mu-controllers and the robust PID increase system resilience. The Mu-controller may be utilized without anti-windup techniques because of its benefits, which include 0 percent overshoot, no oscillations like the robust PID, and no pure integral term. Furthermore, any robust PID and Mu-Controller meet the robustness requirements. The robust PID controller is specifically designed to handle these uncertainties more effectively. It achieved this through using adaptive algorithms that can adjust the control strategy based on real-time conditions. The  $\mu$ -controller design follows a well-defined mathematical framework, making it a systematic and rigorous approach to control system design. This structured approach streamlines the design process and reduces reliance on intuition. This method could be applied to systems of varying complexity, from relatively simple to highly intricate ones. This makes it a versatile tool for a broad range of control problems.

## REFERENCES

- [1] N.D. Manring, " Mapping the Efficiency for a Hydrostatic Transmission," Journal of Dynamic Systems, Measurement, and Control MARCH 2016, Vol. 138 / 031004-1 Copyright V.C. 2016 by ASME.
- [2] Z Jing and Han Qi, " Design and Calculation of Hydraulic Transmission System of Loader," MMEAT 2020 Journal of Physics: Conference Series 1676 (2020) 012242 IOP Publishing, doi:10.1088/1742-6596/1676/1/012242.
- [3] H.H. Ali, and Roger C. Fales, " A review of flow control methods," International Journal of Dynamics and Control (2021) 9:1847–1854 <https://doi.org/10.1007/s40435-020-00730-y>.
- [4] J. Králev, A. Mitov, I. Angelov and T. Slavov " Robust Mu-Controller for Electro-Hydraulic Steering System ", 978-1-5386-9301-8/19/\$31.00 ©2019 European Union
- [5] M. Ba Loc, Hyeung-Sik Choi, Sam-Sang You, and Tae-Woong Um " Mu-synthesis Depth Controller Design for a Small Autonomous Underwater Vehicle," International Symposium on Mechatronics and Robotics, October 26-28, 2011, HCMUT, Vietnam, Conference Paper · January 2011.

DOI: <https://doi.org/10.33103/uot.ijccce.24.3.7>

- [6] N. GUGLIELMI, M.-UR REHMAN, AND D. KRESSNER, "A NOVEL ITERATIVE METHOD TO APPROXIMATE STRUCTURED SINGULAR VALUES" SIAM J. MATRIX ANAL. APPL. 2017 Society for Industrial and Applied Mathematics, Vol. 38, No. 2, pp. 361–386
- [7] A Marcos, P. Rosa, C. Roux, M. Bartolini, and S Bennani, "An Overview of the RFCS Project V&V Framework: Optimization-Based and Linear Tools for Worst-Case Search," CEAS Space Journal, Vol. 7, No. 2, 2015, pp. 303–318.
- [8] N. GUGLIELMI, M.-UR REHMAN AND D. KRESSNER, "A NOVEL ITERATIVE METHOD TO APPROXIMATE STRUCTURED SINGULAR VALUES", SIAM J. MATRIX ANAL. APPL. c 2017 Society for Industrial and Applied Mathematics Vol. 38, No. 2, pp. 361–386.
- [9] A. Mahmood Abdullah, H H. Ali, A A. Al-Qassar, "A ROBUST CONTROLLER DESIGN FOR AN INLET THROTTLING VELOCITY CONTROL SYSTEM FOR A ROTARY ACTUATOR", International Journal of Mechatronics and Applied Mechanics, 2024, Issue 15
- [10] V. Rao, S. Kamath, V. I. George, and C Shreesha "Reliable Robust PID Controller Design for TRMS " Conference Paper · December 2017
- [11] M. G. Skarpetis , F. N. Koumboulis, " Robust PID Controller for Electro - Hydraulic Actuators ", 978-1-4799-0864-6/13/\$31.00 ©2013 IEEE.
- [12] Z. Gosiewski and M. Henzel, " A Robust Controller for Electrohydraulic Drives ", Solid State Phenomena Vol. 113 (2006) pp 61-66 Online available since 2006/Jun/15 at [www.scientific.net](http://www.scientific.net) © (2006) Trans Tech Publications, Switzerland doi:10.4028/www.scientific.net/SSP.113.61
- [13] A. J. Ali, H. H. Abbas and H. Bevrani, " Comparative Analysis of H<sub>2</sub> and H<sub>∞</sub> Robust Control Design Approaches for Dynamic Control Systems", Volume 29 Number 8 August 2023
- [14] S Sami Ali, S. Modher. Raafat and A. Al-Khazraji, " Improving the performance of medical robotic system using H<sub>∞</sub> loop shaping robust controller " Int. J. Modelling, Identification and Control, Vol. 34, No. 1, 2020.
- [15] M. Jibril, M. Tadese and E.Alemayehu Tadese, " Performance Investigation of H<sub>∞</sub> Controller for Quarter Car Semi-active Suspension System Using Simulink " Journal of Information Engineering and Applications", [www.iiste.org](http://www.iiste.org), ISSN 2224-5782 (print) ISSN 2225-0506 (online) Vol.10, No.2, 2019.
- [16] A. H, Fales RC(2020) "Robust control design for an inlet metering velocity control system of a linear hydraulic actuator." Int J Fluid Power. <https://doi.org/10.13052/ijfp1439-9776.2113>.
- [17] A.H, Fales RC, Manring ND (2019) "Modeling and control design for an inlet metering valve-controlled pump that controls actuator velocity via H-infinity and two-degrees-of-freedom methods". <https://doi.org/10.1115/1.4044182>.
- [18] A. Hasan H., M. Firas Abdulsattar, and W.Ahmed. Mustafa. "A New Mechanical Analysis of a Crankshaft-connecting Rod Dynamics Using Lagrange's Trigonometric Identities." Journal of Engineering & Technological Sciences 54, no. 2 (2022).
- [19] M.. Skarpetis and F. N. Koumboulis," Robust PID Controller for Electro - Hydraulic Actuators", 978-1-4799-0864-6/13/\$31.00 ©2013 IEEE.
- [20] M. Skarpetis and F. N. Koumboulis," Robust PID Controller for Electro - Hydraulic Actuators", 978- 1- 4799-0864-6/13/\$31.00 ©2013 IEEE
- [21] V. Vesel'ý, L. Korosi'or'osi," Robust PID controller design for nonlinear systems", Journal of ELECTRICAL ENGINEERING, VOL 69 (2018), NO1, 65–71
- [22] P. Simplício, A. Marcos, X. Lefort," Structured Singular-Value Analysis of the Vega Launcher in Atmospheric Flight", JOURNAL OF GUIDANCE, CONTROL, AND DYNAMICS Aprill, 2016, ORTA DOGO TEKNIK UNIVERSITESI
- [23] D.Wei Gu, P. H. Petkov, M. Mihail. Konstantinov," Robust Control Design with MATLAB," Second Edition.
- [24] J. KraleV, A. Mitov, Tsonyo Slavov and Ilcho Angelov," Robust Mu-Controller for Electro-Hydraulic Steering System", 978-1-5386-9301-8/19/\$31.00 ©2019 European Union
- [25] D.Wei Gu, P. H. Petkov, M. Mihail. Konstantinov," Robust Control Design with MATLAB®",© Springer - Verlag London 2005, 2013, Second Edition